Journal of Physical Science, Vol. 28(2), 85–103, 2017

Visible Light Photocatalytic Activity of $BiFeO_3$ Nanoparticles for Degradation of Methylene Blue

Hajar Atiqah Mohd Azmy, Nor Amirah Razuki, Azia Wahida Aziz, Nurul Syamimi Abdul Satar and Noor Haida Mohd Kaus*

School of Chemical Sciences, Universiti Sains Malaysia, 11800 USM Pulau Pinang, Malaysia

*Corresponding author: noorhaida@usm.my

Published online: 15 August 2017

To cite this article: Mohd Azmy, H. A. et al. (2017). Visible light photocatalytic activity of $BiFeO_3$ nanoparticles for degradation of methylene blue. *J. Phys. Sci.*, 28(2), 85–103, https://doi.org/10.21315/jps2017.28.2.6

To link to this article: https://doi.org/10.21315/jps2017.28.2.6

ABSTRACT: *This study reports on the photocatalytic activity of $BiFeO_3$ nanoparticles on the degradation of cationic dye methylene blue (MB). $BiFeO_3$ prepared by using carrageenan as a biotemplating method were characterised using XRD, SEM and EDX analysis. The effect of different parameters such as catalyst dosage, initial concentration of dye, reaction time, pH, and regeneration study on the removal efficiency were investigated. It was found that 12.79 mmol/L $BiFeO_3$ exhibited 96% degradation of methylene blue at basic pH (pH 8 and pH 10) in 180 min. The catalysts were found to be negatively charged in alkaline medium hence the electrostatic charge attracted more cationic dye towards the catalytic site. Kinetic studies showed the degradation can be described according to Langmuir-Hinshelwood expression.*

Keywords: Bismuth ferrite nanoparticles, methylene blue, biotemplate method, photodegradation, kinetic studies

1. INTRODUCTION

Methylene blue (MB) is one of the organic dyes found in textile industries and generates high effluent that causes environmental pollution. This cationic thiazine dye is very toxic and almost non-biodegradable in nature.[1] The presence of hazardous nondegradable contaminants in water poses dangers for human and environment exposure that result in health effect and environmental damage. Coagulation and flocculation, adsorption on activated carbon, ultrafiltration,

chlorination and ozonation treatment have been proposed to reduce this harmful compound.[2–5] However, all treatments resulted narrow application with short life and requiring high cost. Therefore, some alternative methods which are more cost effective and eco-friendly are required. One of the methods is photocatalytic degradation by inorganic semiconducting catalyst. This method is of great importance in water treatment with rapid and complete oxidation of pollutants in high efficiency.[6]

Inorganic semiconducting catalysts such as TiO_2, ZnO, Fe_2O_3 and CdS have demonstrated their efficiency in degrading a wide range of ambiguous refractory organics into readily biodegradable compounds, and eventually mineralising them to carbon dioxide, water and mineral acids.[7–10] Among all, titanium dioxide (TiO_2) has generated a great interest in research and development of photocatalysis technology due to its potential applications in solar energy conversion inertness to chemical environments, long-term photostability and non-toxicity.[11,12] Nevertheless, TiO_2 can only be activated under UV light irradiation (< 380 nm) due to its wide band gap energy (3.2 eV) for the anatase phase and (3.0 eV) for the rutile phase which limits the effective use of solar energy.[13] This has consequent implications for the use of titania materials as solar or room-light activated catalysts, because majority of solar spectrum consists of 46% visible light and just about 3%–5% of UV light.[14] Therefore, it is of great interest to develop an efficient visible-light photocatalysts for the photo degradation of organic pollutants.

Bismuth ferrite ($BiFeO_3$) is a semiconductor with rhombohedrally distorted perovskite structure. It has narrow band gap of 2.1 eV with high chemical stability which makes it a very good candidate for visible light responsive photocatalytic material.[15] Perovskite-type of $BiFeO_3$ demonstrates the coexistence of multiferroic, ferroelectric and antiferromagnetic properties at room temperature with Neel temperature (TN ~367°C) and Curie temperature (TC ~830°C).[16] It has been reported that synthesis of $BiFeO_3$@carbon core/shell nanofibres with different thickness of carbon layers were successful and are stable under visible light irradiation and could be easily recycled, indicating that they can be used as effective photocatalysts under visible light.[17]

Hydrothermal synthesis of $BiFeO_3$ using KOH concentration of 4 M have been done in order to get the pure phase of bismuth ferrite to increase the photodegradation efficiency.[18] Another method to synthesise bismuth ferrite is by using high purity of Fe_2O_3, Bi_2O_3 and yitrium (III) oxide (Y_2O_3) powders in a conventional solid state reaction technique.[19] Most recently, pure $BiFeO_3$ phase ceramic has also been prepared by a rapid liquid-phase sintering technique.[20,21] Although various approaches have been done to synthesise pure $BiFeO_3$ nanoparticles, it is still

difficult to produce high-purity phase of $BiFeO_3$ as the synthesis of this material is often complex and performed at high temperature (800°C), which leads to the formation of impurity phases (Bi_2O_3, Fe_2O_3 and $Bi_2Fe_4O_9$), poor reproducibility and modified magnetic behaviour.[22] This drawback is usually found in conventional solid state synthesis, sol gel method, mechano-chemical synthesis method and microwave hydrothermal method.[19,23,24] Hence, it is essential to overcome these limitations by synthesising nanostructures of $BiFeO_3$ using a facile synthesis technique that will produce high purity and reproducibility materials.

In the present study, biotemplating technique was used to prepare high-purity $BiFeO_3$ nanoparticles. Biotemplating seeks to either replicate the morphological characteristics and the functionality of a biological/organic species or use a biological/organic structure to guide the assembly of inorganic materials.[25] The surface modification of nanomaterials by biopolymer is also applied to avoid agglomeration, increasing the stability and compatibility in different media.[26] Biotemplating approach is cost effective, less time consuming and environmental friendly as most of the biotemplates are from natural sources.[27]

κ-carrageenan is one of the examples of biological structures that comes from the family of linear sulphated polysachharide and are extracted from red edible seaweeds.[28] The carrageenan also acts effectively to control the size and shape of the nanoparticles. Hydrogel from carrageenan consisting of sulphate ester groups will act as a template for the growth of nanostructures material. This preferential sites will allow the nucleation of the nanoparticles and act as a constrained environment that limits the growth of nanoparticles.[29] Among other established method, a higher calcination temperature of 800°C is used for 5 to 60 min with rapid subsequent cooling. Therefore, biotemplated method was introduced by utilisation of cheap, non-toxic and environmentally friendly materials.

The aim of our study is to synthesise eco-friendly, non-toxic photocatalyst for the degradation of MB under visible light irradiation. The adsorption studies covered the effect of catalyst dosage, pH, initial concentration and contact time, and regeneration study of methylene blue.

2. EXPERIMENTAL

2.1 Materials

Materials used are bismuth nitrate pentahydrate (98% purity) (Sigma-Aldrich, Mexico), iron (III) nitrate nanohydrate (98% purity) (Sigma-Aldrich, Germany),

Sodium hydroxide (QReC), carrageenan (Sigma-Aldrich, USA) and methylene blue ($C_{16}H_{18}CIN_3$) (QReC). All solutions were prepared using distilled water during synthesis.

2.2 Synthesis of $BiFeO_3$

First, 1.4201 g of $Bi(NO_3)_3.5H_2O$ and 2.0202 g of $Fe(NO_3)_3.9H_2O$ were dissolved in 25 mL volumetric flask. 10 mL from the solution was added in 40 mL of 2 wt% (2 g in 200 mL H_2O) carrageenan solution. The pH of the mixture was adjusted until pH 4 using 1.0 M NaOH and dried overnight in oven (80). Finally, the sample was calcined at 550°C for 120 min to yield $BiFeO_3$ powders.

2.3 Characterisation of $BiFeO_3$

The morphology and elemental dispersion on the surface adsorbents were analysed using scanning electron microscope with energy-dispersive X-ray (SEM-EDX) FEI-QUANTA FEG 650. Chromium were used to examine the morphology of the sample. The determination of phase structure and phase purity of sample were analysed using X-ray diffraction (XRD). It was carried out by using a PANalytical X'Pert PRO θ-2θ equipped with graphite monochromatic Cu from 20°C to 70°C at room temperature.

2.4 Adsorption Studies of MB Dye

In order to investigate the MB removal by $BiFeO_3$, batch adsorption studies were conducted under different parameters such as PZC, pH, catalyst dosage, initial dye concentration with contact time, and regeneration of catalyst were carried out. In this batch study, 50 mL of dye solution with 12.787 mmol/L of adsorbents ($BiFeO_3$) were used. After a certain period of time interval, the analytes were centrifuged at 4100 rpm for 20 min and the remaining MB concentration were analysed using Shimadzu 2600 UV Visible spectrophotometer at λ_{max} of 664 nm. The amount of the dye adsorbed at equilibrium, q_e (mg/g) and dye removal (%) of MB were calculated using the following equations:

$$q_e = \frac{(C_o - C_e)V}{m} \tag{1}$$

$$\text{Removal}\,(\%) = \frac{(C_o - C_e)100}{C_o} \tag{2}$$

where C_o (mg/L) is the initial concentration, C_e (mg/L) is the concentration at equilibrium t (min), V (L) is the MB volume and *m* (g) is the mass of adsorbent used.

The pH of point of zero charge (PZC) of pure $BiFeO_3$ determined the pH at which the surface charge is zero. To a series of Erlenmeyer flasks (250 mL), 40 mL of 0.1 M $NaNO_3$ solution was added and the pH of each solution was adjusted to pH 2, 4, 6, 8 and 10 using 0.1 M HNO_3 and 0.1 M NaOH solutions. Then, 6.39 mmol/L of adsorbents were added into each flask and mixtures were left for 24 h at a stirring speed of 250 rpm. The initial (pH_i) and final (pHs) of the suspension was recorded and the change in the pH (ΔpH) was calculated. From the plot of ΔpH versus pH_i, the pH_{pzc} of the adsorbents were determined.

To examine the effect of solution pH on the uptake of MB by $BiFeO_3$, 10 ppm of 50 mL MB at pH 2, 4, 6, 8 and 10 were prepared. The pH was altered by using NaOH and HCl to maintain the required pH condition. To each solution, 12.79 mmol/L of $BiFeO_3$ was added and was left under sunlight for 180 min. After 180 min, the solution was collected and centrifuged to separate the layer from the solid remained.

The effect of catalyst dosage on the MB removal from aqueous solutions was investigated by using various catalyst doses of $BiFeO_3$ as adsorbent which are 3.20 mmol/L, 6.39 mmol/L, 9.59 mmol/L, 12.79 mmol/L and 15.98 mmol/L. In a series of conical flask (250 ml), 50 mL of 10 ppm MB was mixed with adsorbent. All flasks were left under sunlight for 3 h. After 180 min, the solution was collected and centrifuged.

Similarly, to evaluate the effect of concentration and contact time, MB at concentrations 5, 10, 15, 20 and 25 ppm were prepared. Next, 50 mL of each concentration was transferred into a 250 mL conical flask. Afterwards, 12.79 mmol/L $BiFeO_3$ was used for each concentration and then were left under sunlight at different times (30, 60, 90, 120, 150 and 180 min).

Regeneration was done after finishing all the parameters and the best catalyst performance was chosen to be regenerated. The solution of MB loaded with $BiFeO_3$ catalyst was eluted by using 0.1 M HCl as desorbing agents to evaluate the reusability of the MB adsorbents. 12.79 mmol/L $BiFeO_3$ with 50 mL of 10 ppm MB at neutral pH was left under sunlight for 180 min. After that, the concentration of MB in the analyte was determined using Shimadzu 2600 UV visible spectrophotometer at λ_{max} of 664 nm. Then, the catalyst were treated with the desorbing agents by shaking it for 180 min as same duration of reactions

time using orbital shaker Model IKA, KS 260 at 250 rpm. After treatment, the adsorbents were washed with distilled water and re-shake for 180 min and soaked in distilled water overnight. The solid residue was retreated with 50 mL of 10 ppm MB solution for another cycle.

3. RESULTS AND DISCUSSION

3.1 X-ray Diffraction (XRD)

The X-ray diffraction pattern of $BiFeO_3$ nanoparticles confirmed highly crystalline rhombohedral structure (Figure 1). The diffraction peaks for $BiFeO_3$ nanoparticles exist at 2θ values of 22.5°, 32.1°, 39.6°, 46.2°, 51.9°, 57.4° and 67.3°, matching perfectly with the (0 1 2), (1 1 0), (2 0 2), (0 2 4), (1 1 6), (3 0 0), and (2 2 0) crystalline planes of the face rhombohedral structure of $BiFeO_3$ reported in JCPDS 01-073-0548 with average crystallite size of 14.76 nm based on Debye-Scherrer formula. The smaller crystallite size of $BiFeO_3$ nanoparticles prepared by biotemplate method could be attributed to the higher rate of crystal nucleation and growth along the preferential sites of polysaccharide. No corresponding peak of impurities was detected, indicating high purity of the products produced. To confirm the purity of the products, the chemical compositions of $BiFeO_3$ nanoparticles were analysed using EDX spectroscopy. The EDX patterns of nanoparticles are shown in Figure 2(b). The results verify the high purity of the nanoparticles.

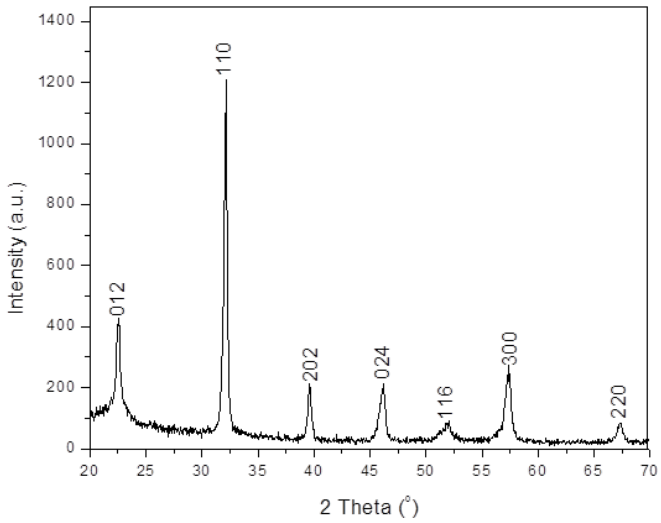

Figure 1: XRD patterns of $BiFeO_3$; JCPDS card no.01-073-0548.

3.2 Scanning Electron Microscope with Energy-dispersive X-ray (SEM-EDX)

The SEM was recorded for surface morphology of $BiFeO_3$ nanoparticles. The shape of the $BiFeO_3$ photocatalytic particles are determined from the obtained images (Figure 2(a)). The SEM photographs revealed synthesised $BiFeO_3$ owing a rhombohedral distorted perovskite structure. EDX pattern of $BiFeO_3$ illustrates patterns of 1% carrageenan at pH 4 as shown in Figure 2(b). The percentage weight of $BiFeO_3$ was found to be of O = 15.37%, Fe = 19.13%, and Bi = 61.95%. The results verify the high purity of the nanoparticles produced.

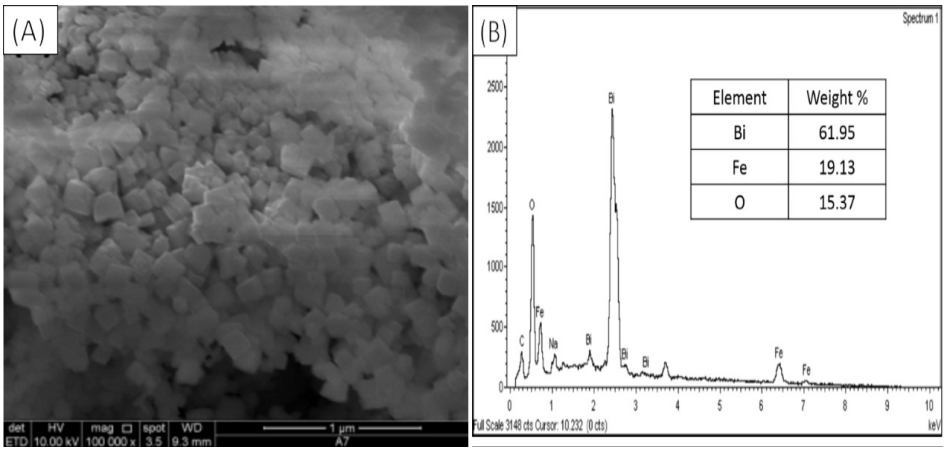

Figure 2: (a) SEM image with magnification of 100,000; (b) EDX result of $BiFeO_3$.

3.3 MB Dye Adsorption Studies

3.3.1 Point of zero charge (PZC)

The pH of the point of zero charge (pH_{pzc}) of $BiFeO_3$ was plotted in Figure 3. The value of pH_{pzc} was determined by the point of intersection from the resulting curve at which the difference between the initial and final pH value was equal to zero. The pH at which the sorbent surface charge takes a zero value is defined as pH_{pzc}. The pH_{pzc} values of $BiFeO_3$ was found to be 8.0. At above pH_{pzc} which is alkaline pHs, the surface of $BiFeO_3$ is negatively charged and could interact with metal positive species.[30] Hence, low amount of MB is adsorbed because the solution contains high concentration of ion hydrogen (H^+) competing with MB ions for exchangeable active sites on $BiFeO_3$. Below the pH_{pzc}, which is acidic pHs, the positive charge of the catalyst surface will repel the MB solution.

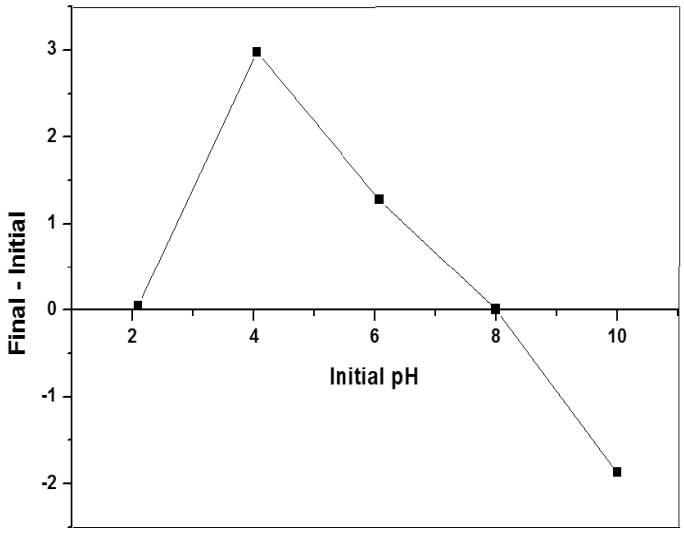

Figure 3: PZC for $BiFeO_3$.

3.3.2 Effect of pH

The effect of pH on the photocatalytic reaction is another important parameter in this study because photocatalytic water treatment is highly dependent on pH as it affects the surface charge of photocatalyst, degree of ionisation as well as active sites of dye molecules.[31] From the graph of PZC, the surface charge of $BiFeO_3$ was found to be positively charged under acidic (H^+) condition and negatively charge under alkaline (OH^-) solution. The percentage degradation of MB increase from lower to higher pH as was showed in Figure 4. Lower percentage of degradation (%) is due to the excess H^+ ion competing with the active sites of cationic dye found at pH 2. Percentage degradation was found to be highest at pH 10 due to negative charges on the surface of $BiFeO_3$ which enhances the positively charged dye cation through electrostatic forces of attraction. Hydroxyl radicals are easily generated by oxidising more hydroxide ions in alkaline solution, thus the efficiency of the process is logically enhanced.[32] Therefore pH 8.0 (basic condition) was chosen to conduct all experiments. From previous research, adsorption at acidic media (pH 2.5 and 3.5) occur in dark (60 min).[33] However, when the pH increased to 6.0, the adsorption and degradation were negligible. The catalyst showed non-adsorption in basic media (8.0, 9.5, 11.0 and 12.0).[33] The comparison of the pH results in dark place and under sunlight showed that that $BiFeO_3$ is best fit to be a photocatalyst and not an adsorbent.

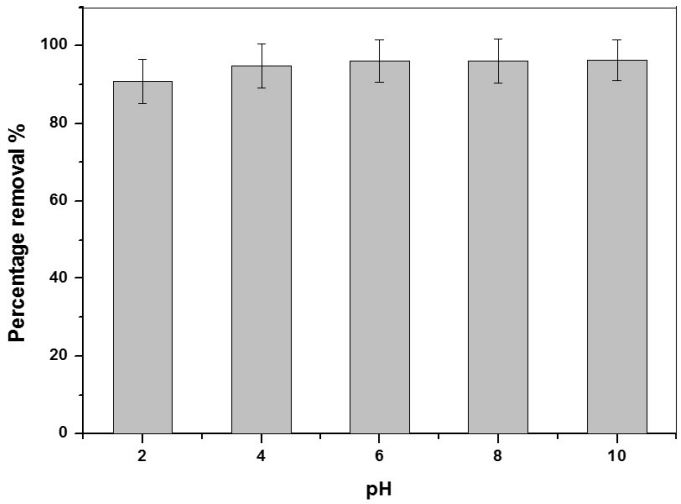

Figure 4: Percentage removal of MB for 180 min vs. pH of 10 ppm MB at neutral pH using 12.78 mmol/L $BiFeO_3$.

3.3.3 Effect of catalyst dosage

Effect of catalyst amount for degradation of dyes was studied in order to acquire an optimised amount of photocatalyst for efficient degradation of pollutants. The photodegradation efficiency (Figure 5) increased as the mass of catalyst dosage increased. This is due to the large number of active sites on the photocatalyst surface, which in turn raised the number of hydroxyl and superoxide radicals that are able to take place in the photocatalysis reaction. In this study, it was found that for 3.20 mmol/L catalyst percentage degradation is 87.80%, 6.39 mmol/L; 94.48%, 9.59 mmol/L; 95.69%, 12.79 mmol/L; 98.92%, and 15.98 mmol/L; 97.60%. From the result, it was shown that the optimum dosage for $BiFeO_3$ in degrading 10 ppm MB is 12.79 mmol/L. Further amount of catalyst added was found to decrease the photodegradation efficiency. This is because the increase in catalyst loading may lead to particle agglomeration and reduced the catalytic activity or it may cause the opaqueness due to scattering of the photons and lead to reduced percentage of removal.[33,34]

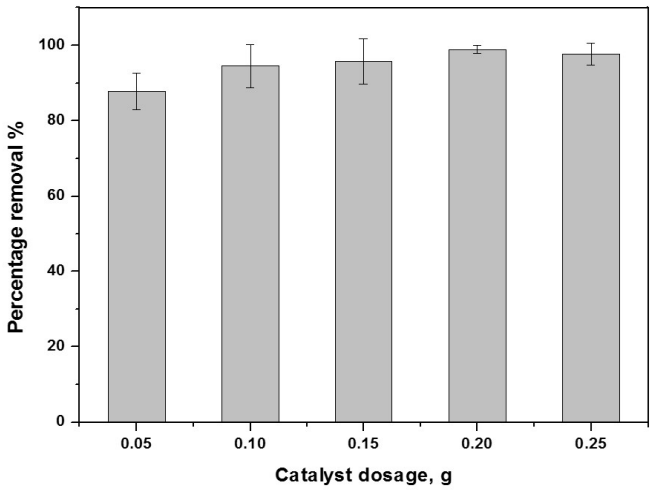

Figure 5: Percentage removal of 10 ppm MB for 180 min at neutral pH vs. $BiFeO_3$ dosage.

3.3.4 Effect of initial concentration and contact time

The effect of initial dye concentration and contact time was studied in the concentration range of 5 ppm to 25 ppm. 12.79 mmol/L $BiFeO_3$ and dye concentration at their neutral pH were used for this study. The results are shown in Figure 6. For 5 ppm, most dyes have successfully degraded during 90 min. While for 10 ppm, most dyes have degraded during 120 min and for 15, 20 and 25 ppm, most dyes have degraded during 150 min. MB solution with higher initial concentration would take relatively longer contact time to attain equilibrium due to the higher amount of MB molecules. The existence of the large amount of adsorbed dye results in the solution to become more intense in colour and the path length of the photons entering the solution decreased, resulting in a few photons reacting on the catalyst surface. Hence, the production of $OH^{\bullet}$ and $OH_2^{\bullet-}$ are reduced and this might have an inhibitive effect on the dye degradation.[35] Moreover, when the initial concentration of dye increased, more dye molecules are adsorbed on the surface of $BiFeO_3$. Hence, it leads to light scattering and as a result will reduce the transmittance of light. From the results obtained, it is clear that the adsorption capacity of the dyes were dependent on the concentration of the dyes.

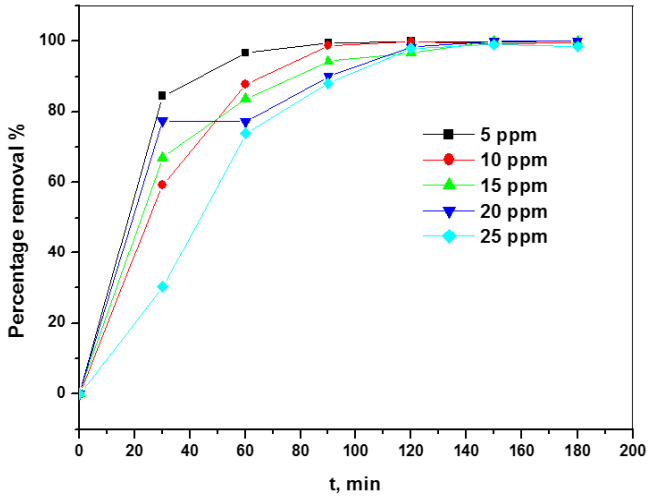

Figure 6: Percentage removal of various concentration of MB at neutral pH vs. contact time using 12.79 mmol/L $BiFeO_3$.

3.4 Mechanism of Photodegradation

The mechanism of the photodegradation of the dyes was also investigated. Advanced oxidation processes (AOPs) is one of the effective means of rapidly treating compounds with efficient process control. Among the new oxidation methods, heterogeneous photocatalysis has proven to be of real interest as an efficient tool for degrading both aquatic and atmospheric organic contaminants.[36] Heterogeneous photocatalysis can be described as the acceleration of photoreaction in the presence of a catalyst and has been carried out to produce hydrogen from water in oxidation reduction reactions using a variety of inorganic semiconductor catalyst materials.[9] When an inorganic semiconductor catalysts irradiate with light energy, an electron (e^-) is excited from the valence band (VB) to the conduction band (CB) of the photocatalyst, leaving a photogenerated hole (h^+). If charge separation is maintained, the electron and hole may migrate to the catalyst surface where they participate in redox reactions with sorbed species. Specially, h^+_{VB} may react with surface bound H_2O or OH^- to produce the hydroxyl radical and e^-_{CB} is picked up by oxygen to generate superoxide radical anion ($O_2^{\bullet-}$). The process of generating $OH^\bullet$ can occur by two pathways, first O_2 present in water is reduced to form O_2^-, which then reacts with H^+ to form $OOH^\bullet$, followed by rapid decomposition to $OH^\bullet$. The second pathway involves the oxidation of OH^- as indicated in the following equations.[33,37]

Absorption of efficient photons by $BiFeO_3$:

$$(BiFeO_3) + hv \rightarrow e^-_{CB} + h^+_{VB} \quad (3)$$

Oxygen ionosorption (first step of oxygen reduction):

$$(O_2)_{ads} + e^-_{CB} \rightarrow O_2^{\bullet -} \quad (4)$$

Neutralisation of OH^- groups by photoholes which produces $OH^\bullet$ radicals:

$$(H_2O \rightarrow H^+ + OH^-)_{ads} + h^+_{VB} \rightarrow H^+ + OH^\bullet \quad (5)$$

Neutralisation of $O_2^{\circ -}$ by photons:

$$O_2^{\circ -} + H^+ \rightarrow HO_2^\circ \quad (6)$$

Rapid decomposition of HO_2° occur and become $OH^\bullet$:

$$2HO_2\cdot + e^-_{CB} \rightarrow OH^- + OH\cdot + O_2 \quad (7)$$

Oxidation of the organic pollutants via successive attack by $OH^\bullet$ radicals:

$$MB + OH^\bullet \rightarrow \text{products } (CO_2 + H_2O + NH_4^+ + SO_4^{2-} + Cl^-) \quad (8)$$

3.5 Langmuir-Hinshelwood (L-H) Model

Langmuir-Hinshelwood (L-H) rate expression has been successfully used for heterogeneous photocatalytic degradation to determine the relationship between the initial degradation rate and the initial concentration of the organic substrate.[38]

$$1/k = (1/ k_c K_{LH}) + ([MB]_0 / k_c) \quad (9)$$

The degradation experiments of MB containing $BiFeO_3$ follow the pseudo-first-order kinetics with respect to the concentration of the dye in the bulk solution. $C = C_0$ at $t = 0$, with C_0 being the initial concentration in the bulk solution and t (the reaction time) will lead to the expected relation:

$$rate = -dC/dt = k_{obs} C \quad (10)$$

where C is the concentration of MB (mg/L) at any time, t is the irradiation time, k is the first-order rate constant of the reaction and K is the adsorption constant of the pollutant on the photocatalyst. This equation can be simplified to a pseudo-first-order equation:[39]

$$C = C_0 e^{-kt} \tag{11}$$

$$\ln (C/C_0) = -k_{obs} \tag{12}$$

where k is first-order rate constant of the photodegradation reaction. According to Equation 12, the plot of ln C/C_0 versus t for all concentrations should be linear and the values of k can be obtained directly via its slope (Figure 7). The obtained values of k are equal to 0.059 min^{-1}, 0.053 min^{-1}, 0.029 min^{-1}, 0.031 min^{-1}, 0.028 min^{-1} for initial concentrations of 5.0 mg/L, 10.0 mg/L, 15.0 mg/L, 20 mg/L, and 25 mg/L, respectively.

Figure 7 shows that the lower MB concentrations provide the better agreement with the first order reaction and have higher value of rate constant. One of the factors of this behaviour is the main steps in the photocatalytic process occur on the surface of the solid photocatalyst.[40] Therefore, a high adsorption capacity is reaction favouring. Because most of the reaction follow L-H equation, this means that at a high initial concentration all catalytic sites are occupied. A further increase in the concentration does not affect the actual catalyst surface concentration and therefore, may result in a decrease in the observed first-order rate constant.[40] In conclusion, the initial concentration of methylene blue has a significant effect on the degradation rates, as the rate constant of degradation is higher when the initial concentration is lower.

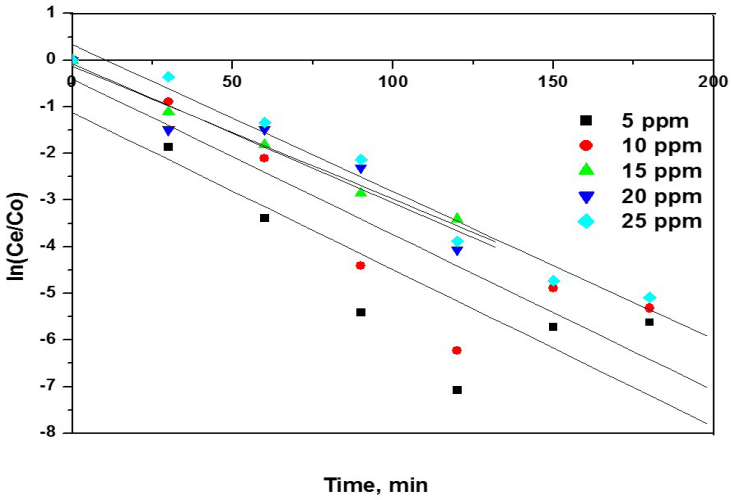

Figure 7: Pseudo first-order L-H model.

3.6 Regeneration of Photocatalyst

In order to investigate the reusability of $BiFeO_3$ nanoparticles in the reaction, the photodegradation experiment was repeated five times. The percentage removal decreased from 97.16% to 37.43% at fifth cycle. From the result showed (Figure 8), after third cycle the photodegradation efficiency become less than 50%. This suggests that there is no significant loss of activity until the third cycle and there is a little loss of activity between fourth and fifth cycle. This trend may be explained by the deposition of organic species on active sites of catalyst, inhibiting its catalytic activity.[41] For cationic dyes, adsorption occurred through electrostatic attraction and hydrogen bond interaction at high solution pH. The surface of the $BiFeO_3$ is positively charged at low solution pH, thus increasing the electrostatic repulsive force between the cationic dyes and the biomass. Therefore, the loaded dyes could be desorbed at acidic conditions. Previous report shows that acid solutions could be used as eluent to regenerate cationic dyes-loaded biosorbent.[42] From the explanation above, it can be concluded that $BiFeO_3$ catalyst successfully degraded MB and can be reused up to third cycle.

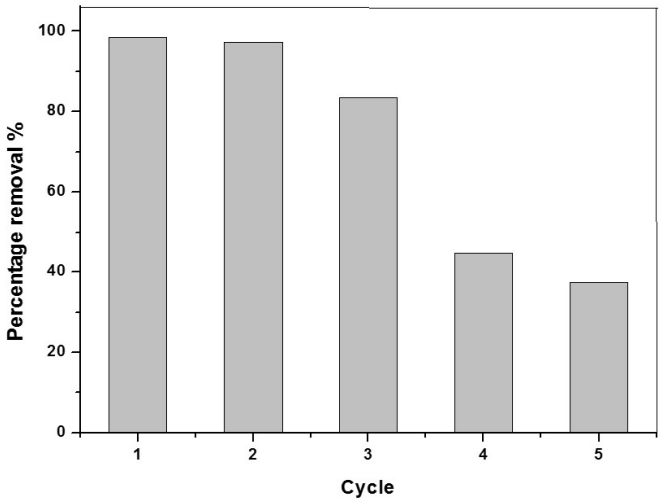

Figure 8: Percentage removal of 10 ppm MB at neutral pH vs. reusability of 12.79 mmol/L $BiFeO_3$.

4. CONCLUSION

In this work, pure $BiFeO_3$ nanoparticles as an effective photocatalyst for the degradation of MB under sunlight irradiation has been successfully synthesised via biotemplate method. XRD results indicated that $BiFeO_3$ was crystallised with single phase of rhombohedrally perovskite distorted structure. PZC values of $BiFeO_3$ was found to be 8.0. The effect of pH was investigated in details in the photocatalysis of MB. The catalyst showed a high adsorption in basic media which is appropriate for the complete degradation at high pH. Different mass of dosage was also investigated to determine the optimum dosage needed to degrade MB dyes. During 90 to 150 min, most of MB dyes starting from 5 to 25 ppm were successfully degraded. Complete removal of MB was observed after visible light irradiation for approximately 180 min. The kinetics of photocatalytics degradation of MB suggested that the kinetic of $BiFeO_3$ photocatalysts follows a pseudo first-order kinetic Langmuir-Hinshelwood model. The $BiFeO_3$ prepared using biotemplate method have shown much better photocatalytic activity in the degradation of MB.

5. ACKNOWLEDGEMENTS

This research was fully supported by Universiti Sains Malaysia Research University (RU) grant, 1001/PKIMIA/811249.

6. REFERENCES

1. Hakam, A. et al. (2015). Removal of methylene blue dye in aqueous solution by sorption on a bacterial-g-poly-(acrylic acid) polymer network hydrogel. *Sains Malays*., 44(6), 827–834, https://doi.org/10.17576/jsm-2015-4406-08.
2. Lee, C. S., Robinson, J. & Chong, M. F. (2014). A review on application of flocculants in wastewater treatment. *Process. Saf. Environ*., 92(6), 489–508, https://doi.org/10.1016/j.psep.2014.04.010.
3. Fathy, N. A., El-Shafey, O. I. & Khalil, L. B. (2013). Effectiveness of alkali-acid treatment in enhancement the adsorption capacity for rice straw: The removal of methylene blue dye. *ISRN Phys. Chem*., Article ID 208087, 1–15, https://doi.org/10.1155/2013/208087.
4. Gupta, V. K. & Suhas. (2009). Application of low-cost adsorbents for dye removal–A review. *J. Environ. Manage*., 90(8), 2313–2342, https://doi.org/10.1016/j.jenvman.2008.11.017.
5. Konstantinou, I. K. & Albanis, T. A. (2004). TiO_2-assisted photocatalytic degradation of azo dyes in aqueous solution: Kinetic and mechanistic investigations: A review. *Appl. Catal. B Environ*., 49(1), 1–14, https://doi.org/10.1016/j.apcatb.2003.11.010.
6. Chong, M. N. et al. (2010). Recent developments in photocatalytic water treatment technology: A review. *Water. Res*., 44(10), 2997–3027, https://doi.org/10.1016/j.watres.2010.02.039.
7. Dozzi, M. V. & Selli, E. (2013). Doping TiO_2 with p-block elements: Effects on photocatalytic activity. *J. Photoch. Photobio. C.*, 14, 13–28, https://doi.org/10.1016/j.jphotochemrev.2012.09.002.
8. Akyol, A., Yatmaz, H. & Bayramoglu, M. (2004). Photocatalytic decolorization of Remazol Red RR in aqueous ZnO suspensions. *Appl. Catal. B Environ*., 54(1), 19–24, https://doi.org/10.1016/j.apcatb.2004.05.021.
9. Ibhadon, A. O. & Fitzpatrick, P. (2013). Heterogeneous photocatalysis: Recent advances and applications. *Catalysts.*, 3(1), 189–218, https://doi.org/10.3390/catal3010189.
10. Peng, T. et al. (2011). Hydrothermal preparation of multiwalled carbon nanotubes (MWCNTs)/CdS nanocomposite and its efficient photocatalytic hydrogen production under visible light irradiation. *Energ. Fuel*., 25(5), 2203–2210, https://doi.org/10.1021/ef200369z.

11. Yang, Y. et al. (2014). Quick and facile preparation of visible light-driven TiO_2 photocatalyst with high absorption and photocatalytic activity. *Sci. Rep. UK*, 4(1), 1–7, https://doi.org/10.1038/srep07045.
12. Akpan, U. & Hameed, B. (2009). Parameters affecting the photocatalytic degradation of dyes using TiO_2-based photocatalysts: A review. *J. Hazard. Mater.*, 170(2), 520–529, https://doi.org/10.1016/j.jhazmat.2009.05.039.
13. Lin, H. et al. (2006). Size dependency of nanocrystalline TiO_2 on its optical property and photocatalytic reactivity exemplified by 2-chlorophenol. *Appl. Catal. B Environ*., 68(1), 1–11, https://doi.org/10.1016/j.apcatb.2006.07.018.
14. Seery, M. K. et al. (2007). Silver doped titanium dioxide nanomaterials for enhanced visible light photocatalysis. *J. Photoch. Photobio. A.*, 189(2), 258–263, https://doi.org/10.1016/j.jphotochem.2007.02.010.
15. McDonnell, K. A. et al. (2013). Photo-active and optical properties of bismuth ferrite ($BiFeO_3$): An experimental and theoretical study. *Chem. Phys. Lett*., 572, 78–84, https://doi.org/10.1016/j.cplett.2013.04.024.
16. Freitas, V. F. et al. (2013). Structural phase relations in perovskite-structured $BiFeO_3$-based multiferroic compounds. *J. Adv. Ceram*., 2(2), 103–111, https://doi.org/10.1007/s40145-013-0052-2.
17. Liu, Y., Zuo, R. & Qi, S. (2013). Controllable preparation of $BiFeO_3$@carbon core/shell nanofibers with enhanced visible photocatalytic activity. *J. Mol. Catal. A Chem*., 376, 1–6, https://doi.org/10.1016/j.molcata.2013.04.005.
18. Ponzoni, C. et al. (2013). Optimization of BFO microwave-hydrothermal synthesis: Influence of process parameters. *J. Alloy. Compd*., 558, 150–159, https://doi.org/10.1016/j.jallcom.2013.01.039.
19. Gómez, J. M. et al. (2016). Structural study of yttrium substituted $BiFeO_3$. *J. Phys. Conf. Series.*, 687(1), 1–4.
20. Pradhan, A. K. et al. (2005). Magnetic and electrical properties of single-phase multiferroic $BiFeO_3$. *J. Appl. Phys*., 97(093903), 1–5, https://doi.org/10.1063/1.1881775.
21. Awan, M. & Bhatti, A. (2009). Room-temperature multi-ferrocity in off-stoichiometric $Bi_{1.1}FeO_3$ ceramics prepared by melt-phase sintering. *Nucleus*., 46(4), 465–471.
22. Maurya, D. et al. (2009). $BiFeO_3$ ceramics synthesized by mechanical activation assisted versus conventional solid-state-reaction process: A comparative study. *J. Alloy. Compd*., 477(1), 780–784, https://doi.org/10.1016/j.jallcom.2008.10.155.
23. Johari, A. (2011). Synthesis and characterization of bismuth ferrite nanoparticles. *AKGEC J. Technol*., 2(2), 17–20.
24. Gao, T. et al. (2015). A review: Preparation of bismuth ferrite nanoparticles and its applications in visible-light induced photocatalyses. *Rev. Adv. Mater. Sci*., 40, 97–109.

25. Sotiropoulou, S. et al. (2008). Biotemplated nanostructured materials. *Chem. Mater*., 20(3), 821–834, https://doi.org/10.1021/cm702152a.
26. Ramimoghadam, D., Bagheri, S. & Abd Hamid, S. B. (2014). Biotemplated synthesis of anatase titanium dioxide nanoparticles via lignocellulosic waste material. *Biomed. Res. Int*., 1–7, https://doi.org/10.1155/2014/205636.
27. Selvakumar, R. et al. (2014). Recent advances in the synthesis of inorganic nano/microstructures using microbial biotemplates and their applications. *RSC. Adv*., 4(94), 52156–52169, https://doi.org/10.1039/C4RA07903E.
28. Campo, V. L. et al. (2009). Carrageenans: Biological properties, chemical modifications and structural analysis – A review. *Carbohyd. Polym*., 77(2), 167–180, https://doi.org/10.1016/j.carbpol.2009.01.020.
29. Trindade, T. & da Silva, A. L. D. (Eds). (2011). *Nanocomposite particles for bio-applications: Materials and bio-interfaces*. New York: Taylor & Francis Group.
30. Fiol, N. & Villaescusa, I. (2009). Determination of sorbent point zero charge: usefulness in sorption studies. *Environ. Chem. Lett*., 7(1), 79–84, https://doi.org/10.1007/s10311-008-0139-0.
31. Auta, M. & Hameed, B. (2014). Chitosan–clay composite as highly effective and low-cost adsorbent for batch and fixed-bed adsorption of methylene blue. *Chem. Eng. J*., 237, 352–361, https://doi.org/10.1016/j.cej.2013.09.066.
32. Li, J. et al. (2008). Adsorption and degradation of the cationic dyes over Co doped amorphous mesoporous titania-silica catalyst under UV and visible light irradiation. *Micropor. Mesopor. Mat*., 115(3), 416–425, https://doi.org/10.1016/j.micromeso.2008.02.022.
33. Soltani, T. & Entezari, M. H. (2013). Photolysis and photocatalysis of methylene blue by ferrite bismuth nanoparticles under sunlight irradiation. *J. Mol. Catal. A Chem*., 377, 197–203, https://doi.org/10.1016/j.molcata.2013.05.004.
34. Muruganandham, M. & Swaminathan, M. (2006). Photocatalytic decolourisation and degradation of reactive orange 4 by TiO_2-UV process. *Dyes. Pigments*., 68(2), 133–142, https://doi.org/10.1016/j.dyepig.2005.01.004.
35. Khataee, A., Vatanpour, V. & Ghadim, A. A. (2009). Decolorization of CI Acid Blue 9 solution by UV/Nano-TiO_2, Fenton, Fenton-like, electro-Fenton and electrocoagulation processes: A comparative study. *J. Hazard. Mater*., 161(2), 1225–1233, https://doi.org/10.1016/j.jhazmat.2008.04.075.
36. Salehi, M., Hashemipour, H. & Mirzaee, M. (2012). Experimental study of influencing factors and kinetics in catalytic removal of methylene blue with TiO_2 nanopowder. *Am. J. Environ. Eng*., 2(1), 1–7, https://doi.org/10.5923/j.ajee.20120201.01.

37. Gaya, U. I. & Abdullah, A. H. (2008). Heterogeneous photocatalytic degradation of organic contaminants over titanium dioxide: A review of fundamentals, progress and problems. *J. Photoch. Photobio. C.*, 9(1), 1–12, https://doi.org/10.1016/j.jphotochemrev.2007.12.003.
38. Khezrianjoo, S. & Revanasiddappa, H. (2012). Langmuir-Hinshelwood kinetic expression for the photocatalytic degradation of Metanil Yellow aqueous solutions by ZnO catalyst. *Chem. Sci. J.*, 3, 1–7.
39. Mijin, D., Radivojević, J. & Jovančić, P. (2007). Photocatalytic degradation of textile dye CI Basic Yellow 28 in water by UV-A/TiO_2. *Chem. Ind. Chem. Eng. Q.*, 13(1), 33–37, https://doi.org/10.2298/CICEQ0701033M.
40. Anpo, M. & Kamat, P. V. (2010). *Environmentally benign photocatalysts: applications of titanium oxide-based materials*. New York: Springer Science & Business Media, https://doi.org/10.1007/978-0-387-48444-0.
41. Siddiqa, A. et al. (2015). Cobalt and sulfur co-doped nano-size TiO_2 for photodegradation of various dyes and phenol. *J. Environ. Sci.*, 37, 100–109, https://doi.org/10.1016/j.jes.2015.04.024.
42. Vijayaraghavan, K. et al. (2008). Chemical modification of Corynebacterium glutamicum to improve methylene blue biosorption. *Chem. Eng. J.*, 145(1), 1–6, https://doi.org/10.1016/j.cej.2008.02.011.